FLOMEKO 2003
11th IMEKO TC9 Conference on Flow Measurement
Groningen, NETHERLANDS, 12 - 14 May 2003

Influence of Shape Deviations on the Measurement Precision of Vortex Flow Meters

Ernst von Lavante, Institute of Turbomachinery, University of Essen, Essen, Germany
Burger Nath, ABB Automation Products GmbH, Goettingen , Germany

Abstract - In the present investigation, the problem of accurate determination of volumetric flows by means of the so-called vortex-shedding flow meter in the case of shape changes and deviations of the geometry from the original specifications due to manufacturing tolerances and imperfections was studied. To this end, the flow about the bluff body used in the presently studied vortex-shedding flow meter was numerically simulated using a solver of the unsteady, compressible (air) or incompressible (water) Navier-Stokes equations in two and three dimensions. The computations were carried out for several types of modified geometry including a slightly rotated bluff body, rounded edges representing wear and asymmetrically oriented sensor body called here “paddle”. The results were compared, where possible, with experimental data obtained by the manufacturer. The effects of turbulence were modeled by using the realizable k-ε turbulence model. The resulting flow fields were analyzed using various methods, including visualization, evaluation of several of their global features and DFT of properly chosen variables.

Introduction

Many chemical and environmental processes found in the corresponding industries require volume- or mass flow data for their completion. Number of promising new methods for flow rate measurement have been recently developed. One relatively simple flow measurement device is the so-called vortex-shedding flow meter, in which the volume flow is determined by observing the relationship between the vortex-shedding frequency from a bluff body attached inside a channel, and the corresponding mean velocity about it. The bluff body causes production of a system of periodic vortices (vortex street), whose frequency can be correlated with the mean flow velocity and, therefore, the volume flow. This procedure assumes a regular and well defined vortex structure as well as shedding mechanism, resulting mostly in linear dependency of the volumetric flow on the shedding frequency over a wide range of Reynolds numbers.
Commercial flow meters use a large variety of bluff body shapes, often restricted by the attachment of the pressure sensors or, more likely, the patent laws. In the past, various shapes of vortex bodies have been tested with regard to their applicability to a simple signal processing. Triangular shapes (Johnson [4], Fureby [1] and Madabhushi et. al. [5]) as well as shapes with truncated tips (e. g. Hans et. al. [2] and [3]) have been tested. Previous application of some currently manufactured bluff body designs lead to fairly irregular pressure signatures, making them unreliable. In the preliminary part of this work (von Lavante et al. [6]), tests were performed with T-shaped, rectangular and newly designed bluff bodies. Well-defined vortices were generated, giving, after signal processing, excellent measurement results. A strong and well-defined dependency of the vortex frequency on the flow velocity and, therefore the Reynolds number, could be obtained.
It has been also observed that a slight uncontrolled modification of the assumed geometry a particular vortex-shedding flow meter, e.g. shape and location relative to the surrounding casing, could cause a shift of its characteristic frequencies, leading to unreliable volumetric flow data. The aim of the present research was the investigation of these effects.

Principle of vortex-shedding meters

In principle, the vortex-shedding flow meters use the separation frequency of vortices behind a bluff body to measure the mean flow velocity of a fluid flow. Downstream of the bluff body, a von Karman vortex street develops; its width d and distance T between the vortices depends on this frequency f, and therefore on the bluff body's shape. A typical configuration of this type of flow meter is shown in principle in Fig. 1. Preferably, the vortex-shedding frequency should depend linearly on the mean flow velocity for a wide Reynolds number range. The dependency of the vortex frequency f, the mean flow velocity u_m and the width of the bluff body d is expressed by the dimensionless Strouhal number Sr:

$$Sr = (d \cdot f)/u_m.$$

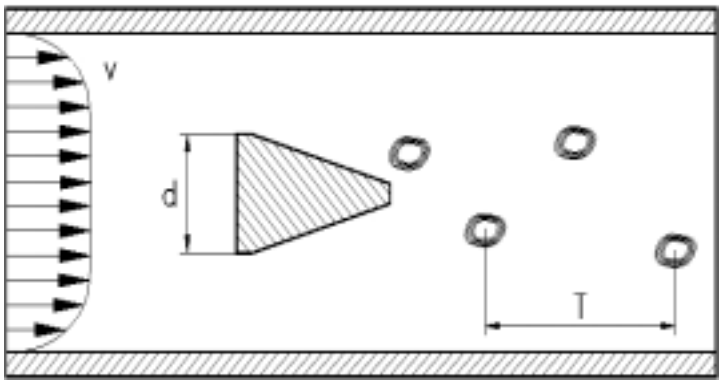

Figure 1. Principle of a vortex-shedding flow meter.

Usually, the detection of the vortices is carried out by pressure sensors inside the bluff body. The vortex structures can also be detected by an ultrasound barrier behind the body, as implemented by, for example, Hans et al. [2].
The present flow meter, manufactured by ABB Automation Products, is using rather a simple yet effective method of detecting the vortices shed by the bluff body. A second much smaller body was installed behind the main bluff body, protruding from the wall almost to the centre of the meter. The meter then correlates the frequency of oscillation of the bending moment exerted on this paddle to the flow rate. The main advantage of this arrangement is its integrating characteristic (it measures the integral of the pressure on its surface), resulting in a rather smooth signal, as can be seen in Fig. 7. The geometry as considered in the present work is displayed in Fig. 2. Here, the outer casing (piping) has been removed in order to show the shape and position of the bluff body and the paddle. The test section selected for the present studies had a diameter of 50 mm (DN50).

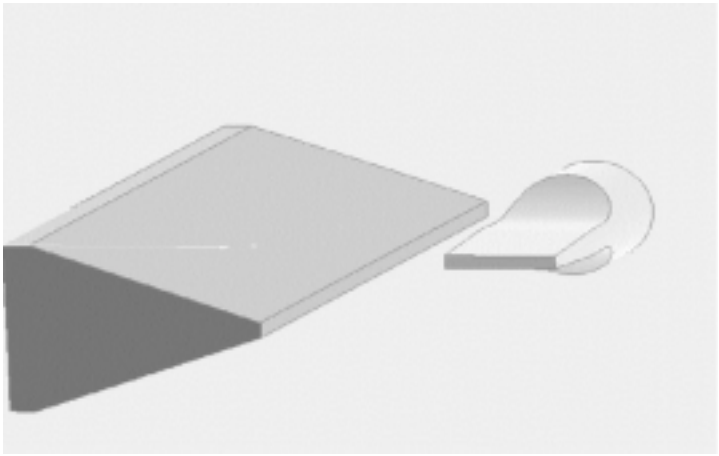

Figure 2. Geometry of the bluff body and paddle used for measuring the vortex-shedding frequency.

Numerical method

In the present work, the flow was investigated using a commercially available Navier-Stokes equations solver, the FLUENT system of programs Version 6.xx, capable of handling unsteady, compressible and incompressible viscous flows over a wide range of applications. In all simulations, the realizable k-ε turbulence model was applied.
Close attention was paid to the formulation of the inflow and outflow boundary conditions, as these had to be perfectly nonreflective. The best results were obtained in the case of compressible flows using the pressure far-field inlet boundary and pressure outlet boundary. All the other boundary conditions available in FLUENT gave inferior results. In particular, the widely used velocity inlet boundary condition, which specifies the velocity, resulted in a perfectly steady flow! In the case of incompressible flow, the above boundary conditions can not be used. Here, the velocity specifying inlet boundary had to be selected. As this boundary condition is perfectly reflecting, something had to be done in order to avoid spurious waves being trapped in the computational domain. The authors had to devise a “dump” region of high numerical viscosity far downstream of the bluff body to damp out these waves.

The standard fully developed turbulent profile due to Nikuradse was implemented in the inflow. The segregated solver was used in its second-order accurate implicit form. The computations were compared with global experimental results consisting mainly of very accurately measured vortex shedding frequencies.

Basic configuration

Since a typical fully three-dimensional simulation of the configuration shown in Fig. 2 requires in excess on 10^6 cells and therefore several computational weeks, it was decided to first investigate several configurations in two dimensions. The two-dimensional configuration assumed in the present work can be seen in Fig. 3. It consists of projection of the bluff body and the paddle, oriented downstream of it.

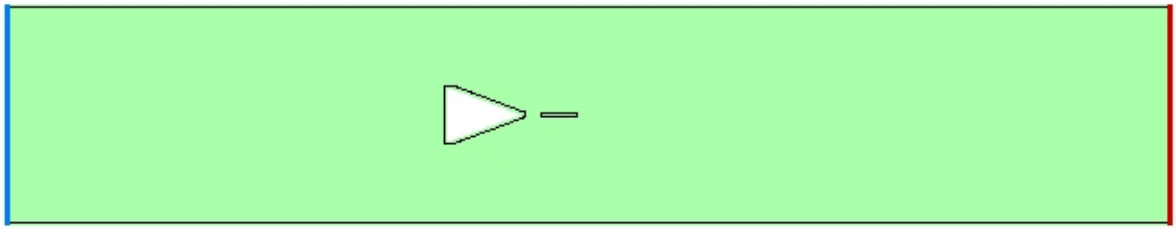

Fig. 3. Basic configuration studied.

A structured computational grid consisting of more than 40.000 cells arranged in 10 blocks was generated. Close attention was paid to the grid resolution in critical areas such as boundary layers. A part of the grid about the two bodies is displayed in Fig. 4 for the basic configuration according to the designer's plans.

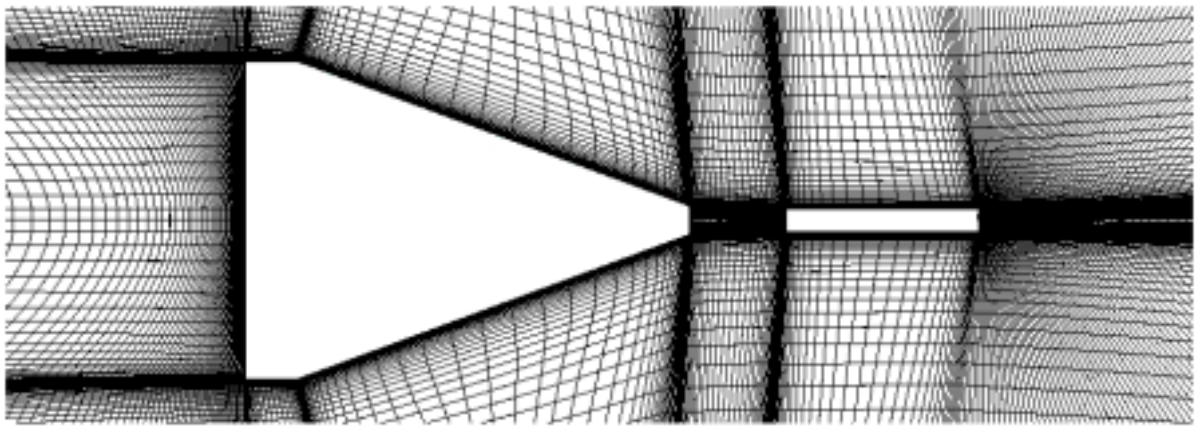

Fig. 4. Partial view of the computational grid for the basic configuration.

Even in the two-dimensional case, the convergence to the correct solution required several days on a 2 GHz PC. A momentary static pressure distribution for a maximum mean flow velocity given by u_m= 65 m/s can be found in Fig. 5. At this mean flow velocity, the Reynolds number was $Re=57 \cdot 10^3$. Recognizable is not only a strong primary vortex just passing over the paddle, but also a second primary vortex being generated at the lower part of the rear portion of the bluff body. As the typical von Karman vortex street develops, this second vortex alternates between the upper and lower surfaces of the bluff body.
Interestingly, there is a fairly strong flow in direction perpendicular to the main flow between the two bodies. A further primary vortex is just passing out of the view.

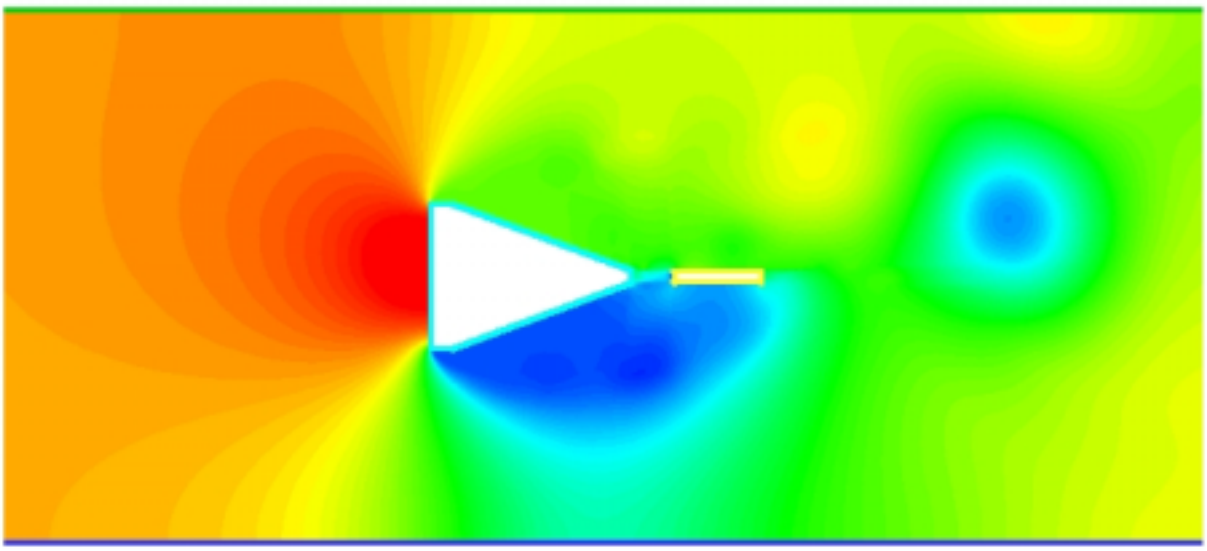

Fig. 5. Static pressure at the bluff body and the paddle.[1]

The computed unsteady force in vertical direction (called from now on lift) on the paddle (second body) is shown in Fig. 6. In this and all the subsequent figures, the lift force is shown in N/m since the flow was assumed to be two-dimensional. The predicted lift displays satisfyingly regular shape. The results of a DFT-transformation using the Hanning filter can be viewed in Fig. 7 in the frequency domain. Accordingly, the lift displays a clean peak in the frequency domain, Fig. 7.

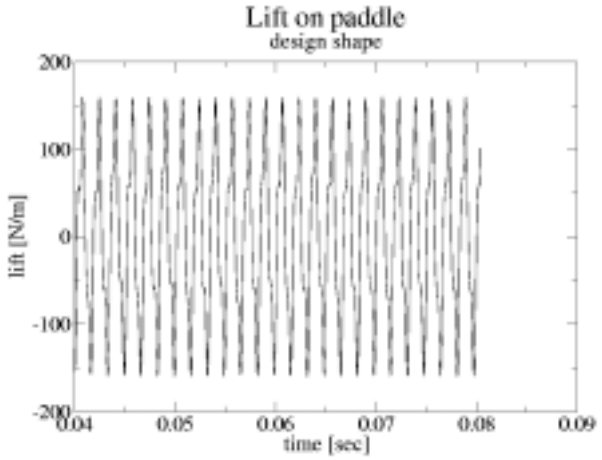

Fig. 6. Lift force on the paddle (second body).

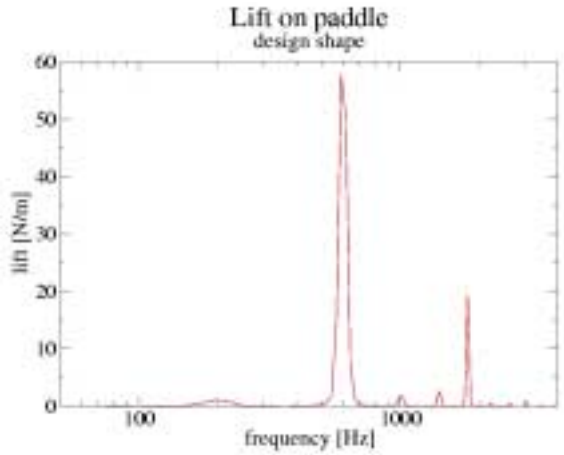

Fig. 7. DFT-transformation of the lift force.

The resulting dominating frequency of 593 Hz agrees rather well with the measured frequency of 590 Hz. The corresponding Strouhal Number is Sr =0.1220, being within 0.5% of the measured value. The present two-dimensional simulation was not able to recover the degree of linearity measured experimentally. This is to be expected, since the assumed shape in Fig. 3 is trying to model the configuration in Fig. 2. The paddle extends in reality approximately to the centerline, causing at its tip severe three-dimensional effects. The dependency of the Strouhal number Sr on the Reynolds number Re can be viewed in Fig. 19. For larger Reynolds numbers and, therefore, larger mean flow velocities the Strouhal number remains constant within approximately 2.5 %, which is again in good agreement with the experiments. At the smallest Reynolds number, corresponding to an inflow velocity of about u_m = 33 m/s, the assumption of compressible flow is at its limits. In particular, the inflow boundary condition is strictly valid only for compressible flows,

[1] Two video clips showing the unsteady flow field are included on the CD in the avi-format. Their names are vortex_flow_meter1.avi and vortex_flow_meter2.avi

e.g. for Mach numbers in access of approximately M=0.15. This tendency can be recognized in all cases simulated in the present work.

Shifted Paddle

One possible deviation from the designed shape can occur when the second body (paddle) is installed slightly above the centerline of the bluff body. The present authors call this case ”the shifted paddle”. For the purpose of simulations, the paddle was translated by 1 mm in the vertical direction, see Fig. 8. This relatively small imperfection had a strongly negative effect on the time wise signature of the lift.

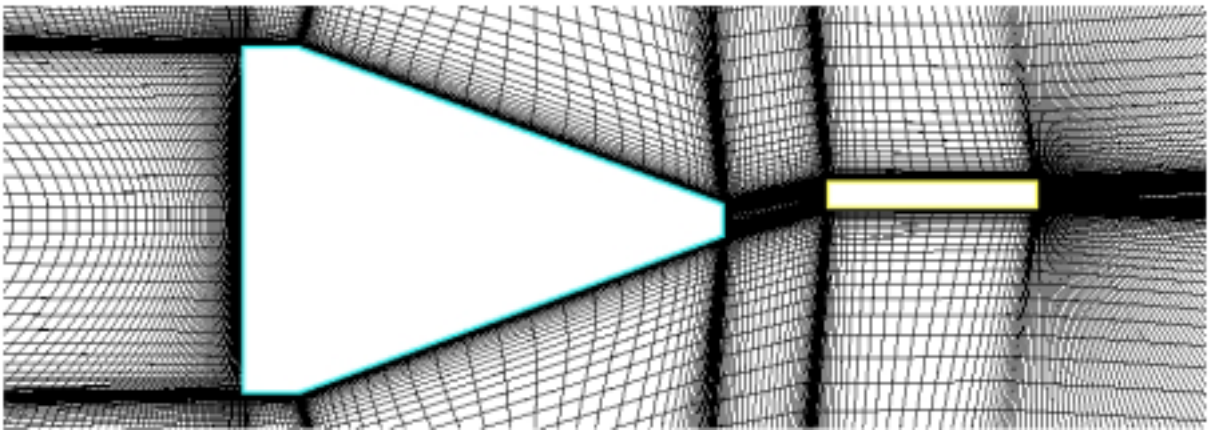

Fig. 8. Computational grid showing the shifted paddle.

As can be seen in Fig. 9, the signal coming from the paddle is very irregular - a nightmare for signal processing. The time wise fluctuation of the lift is not centered about zero, but experiences a steady negative component. The paddle displays several separation points, resulting in a very complex pressure distribution along its surface. Typical static pressure contours are shown in Fig. 11. Surprisingly, after performing DFT with the Hanning filter, there is a dominating frequency that actually is within 7.5 % from the measured value and displays a clean peak in the frequency domain. The result of the DFT is presented in Fig. 10. Although the dominating peak is not as well defined as in the design case, it is distinguishable. Again, the linearity is maintained for larger velocities.

The flow field offers some rather interesting features. A detailed view of the flow near the two bodies reveals that there is separation in two locations on the paddle, the front side due to reversed flow and on the upper rear surface due to the primary vortex above it. The time wise history of the pressure is even more exciting.

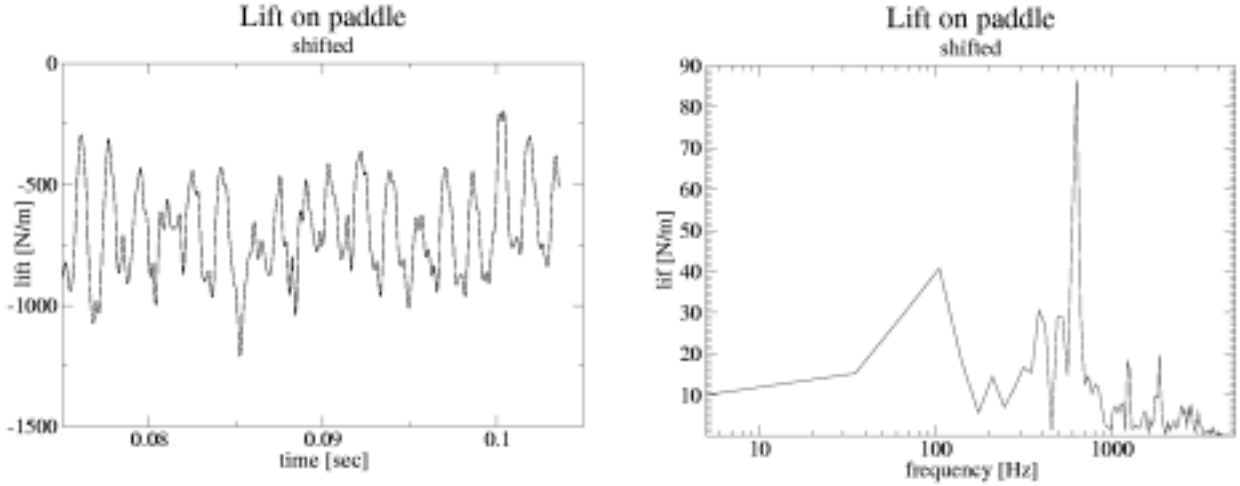

Fig. 9 and 10. Lift force on second body for the case of shifted paddle and results of DFT.

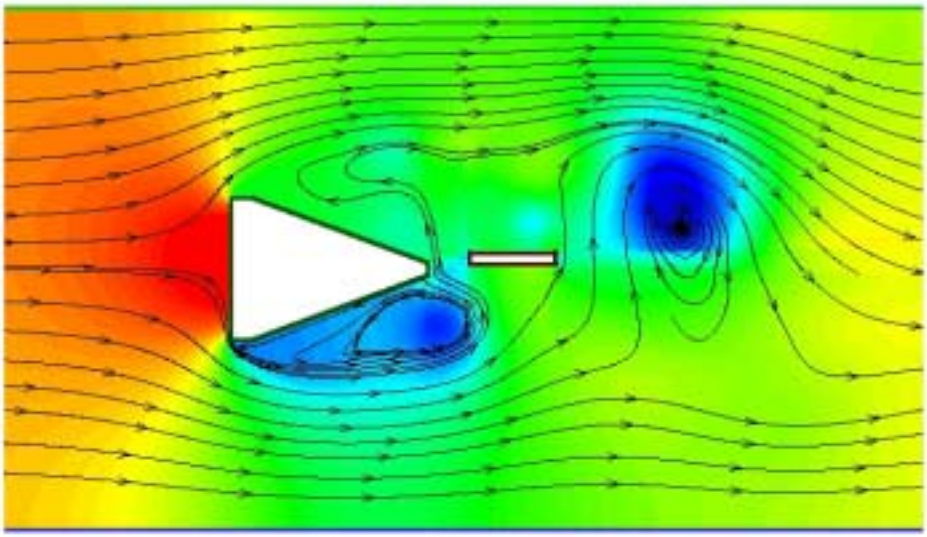

Fig. 11. Static pressure distribution and streamlines.

In Fig. 12, the flow field near the paddle is shown. At this particular instant, an upper primary vortex located downstream of the paddle induces flow normal to the surface of the paddle from the bottom to the top. The fluid streams around the body, being separated at the sharp edges. In particular, the separation bubble at the trailing edge is noticeable. A secondary vortex is formed above the paddle, causing one of the irregularities in the time wise history of the lift force. The secondary vortex is remarkably regular in shape. Upstream of it, there is another rather vortex structure, generated by the circulation of the separated fluid. The above details were captured due to the fairly high resolution used in the present work.

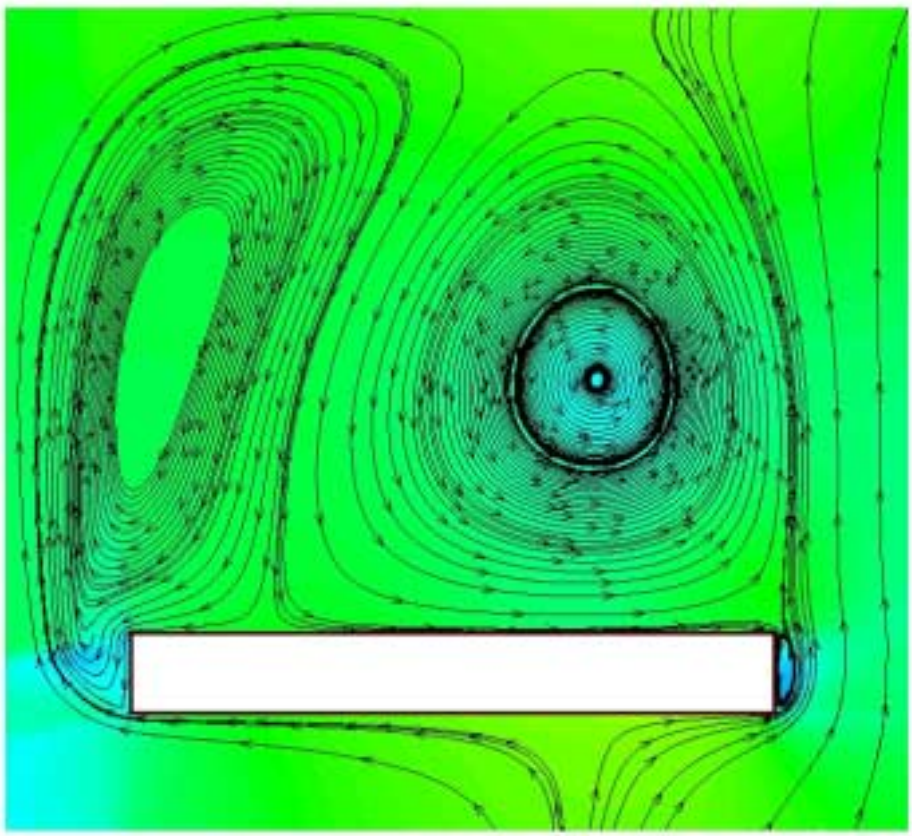

Fig. 12. Static pressure distribution and streamlines on the second body.

Rotated bluff body

The effects of inaccurately installed bluff bodies were simulated assumed that it was rotated about an imaginary axis located in the centre of the front side facing the flow. Two rotation angles were implemented, 1^o and 2^o. The corresponding grid can be viewed in Fig. 13.

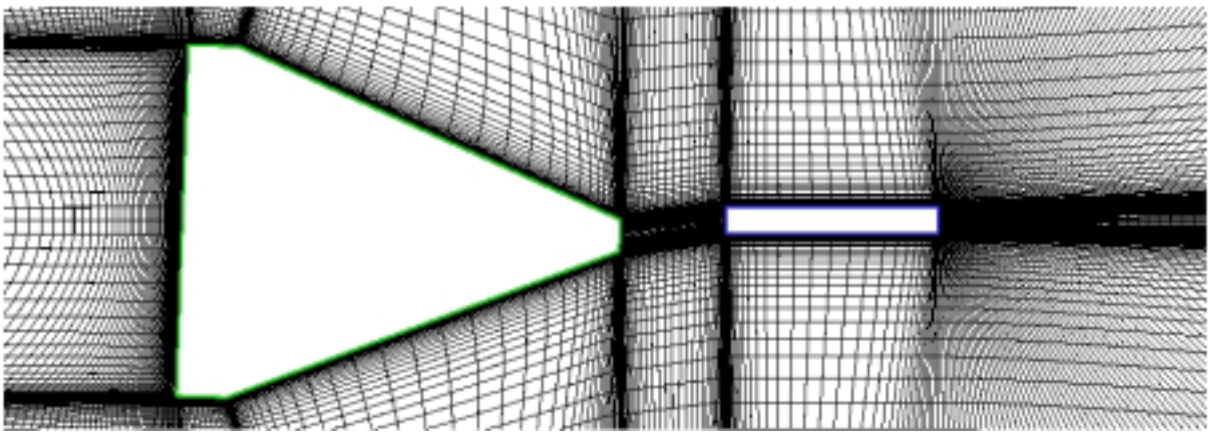

Fig. 13. Grid about the bluff body rotated by 2 degrees.

The resulting signal given by the paddle is displayed in Fig. 14. The signal is still relatively clean, with a noticeable modulation of its amplitude at a lower frequency. At 2 degrees rotation, there is a shift in the dominant frequency, but again, the peak in the frequency domain is clean. Proper calibration could restore the accuracy of the meter. At higher degrees of rotation, the quality of the signal deteriorates significantly until, in extreme cases, one of the primary vortices would be missing altogether.

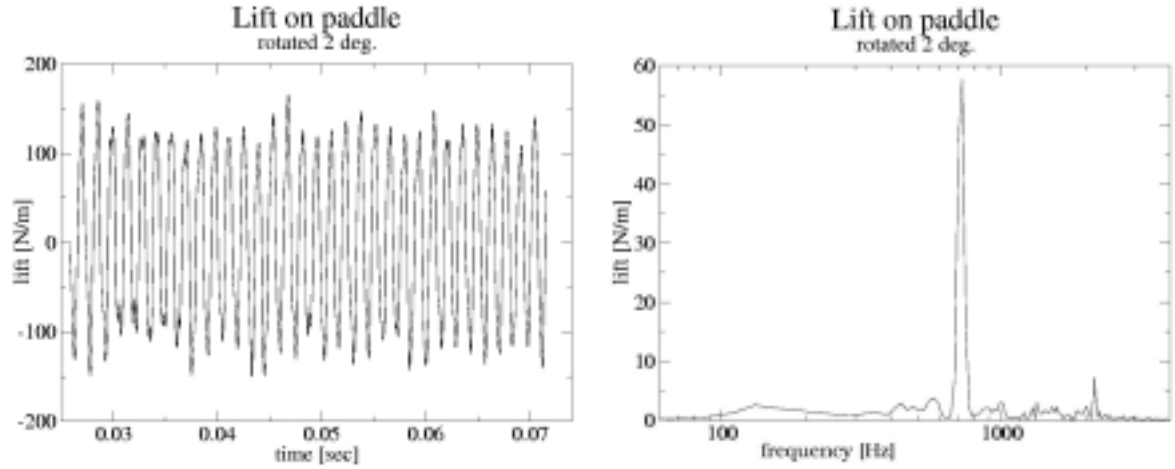

Fig. 14 and 15. Lift force on the paddle for rotated bluff body and results of DFT.

The resulting dominating frequency is in this case much larger than the undisturbed frequency, as can be seen in Fig. 15.

A plausible explanation can be gained by considering Fig. 16. Here, a detailed view of the flow field is given in terms of contours of static pressure and stream lines. The pressure is displayed as gauge pressure in Pa relative to the ambient pressure of $1.01325\ 10^5$ Pa.
A primary vortex just left the upper surface of the bluff body and travels downstream. It induces a strong downstream component of the velocity, generating a secondary vortex below the paddle. Due to the offset of the tip of the bluff body, there is a significant backflow between the two bodies, causing massive separation. This in turn will result in different flow patterns and, therefore, change in frequency of the lift fluctuation. Below the bluff body, further primary vortex is about to separate from the surface.

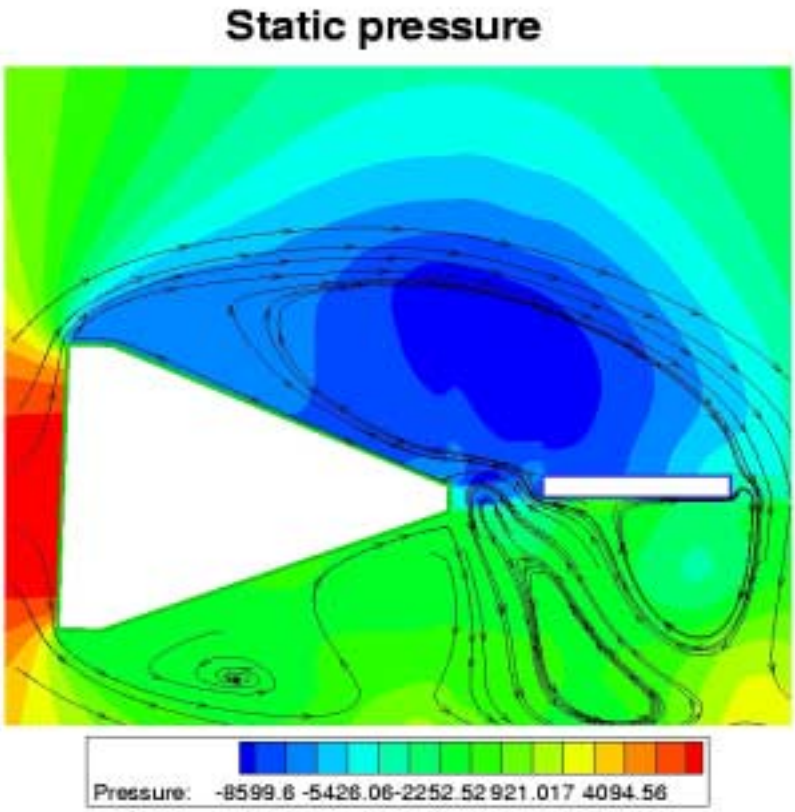

Fig. 16. Static pressure and streamlines for the rotated bluff body.

Three-dimensional Results

As there are significant three-dimensional effects expected in the present configuration, it was decided to simulate the corresponding flow field. In a preliminary study, the flow field about a separate bluff body was predicted using a fairly coarse grid of approximately $200 \cdot 10^3$ cells. After gaining some experience, the grid was refined to approximately $5 \cdot 10^5$ grid cells in a grid shown in Fig. 17. It consisted of 24 blocks of structured grid in order to allow high resolution while maintaining good accuracy in viscous shear layers.

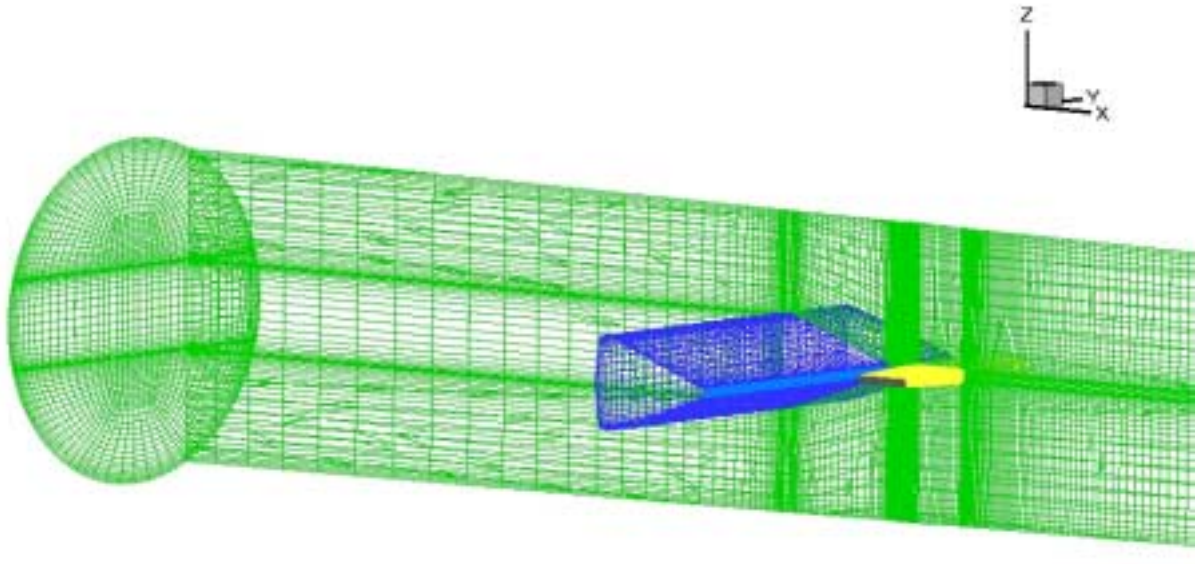

Fig. 17. View of the three-dimensional grid.

The surface grid was exponentially stretched to allow high resolution at the leading and trailing edges. The resulting flow field displaying contours of constant density can be viewed in Fig. 18.

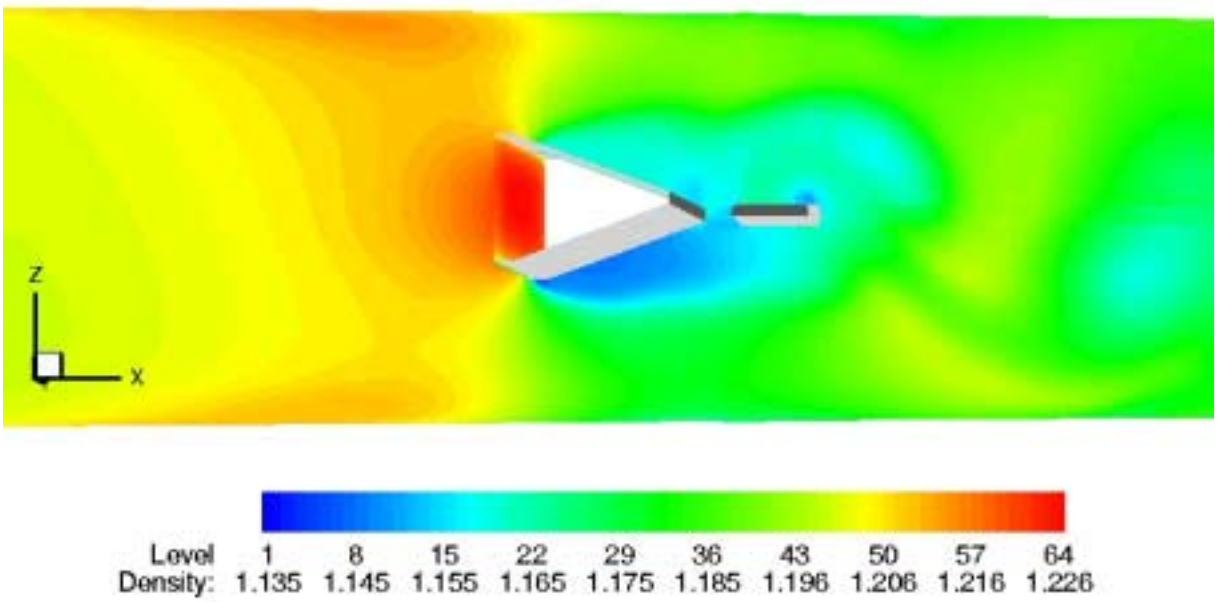

Fig. 18. Three-dimensional flow field near the bluff body and paddle visualized by contours of constant density.

Clearly visible is the bluff body with its stagnation face pointing upstream and a primary vortex just separating from the lower surface. As in the two-dimensional simulations, a secondary vortex at the trailing edge of the paddle can be detected as an area of low density. The flow has at this a mainly two-dimensional character. This would explain why the two-dimensional results were in reasonable agreement with the experimental data, as can be seen in Fig. 19. Further downstream, the vortices were deformed by the non-uniform velocity distribution near the pipe walls.

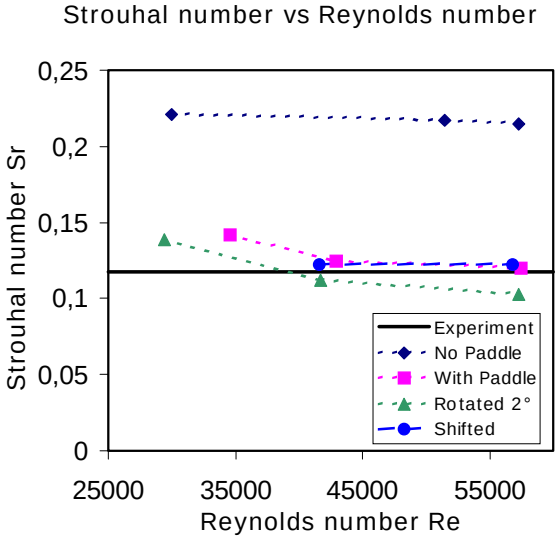

Fig. 19. Strouhal number vs. Reynolds number for different cases as a comparison with the experiment.

The resulting Strouhal numbers Sr shown as a function of the Reynolds number Re based on different configurations is displayed in Fig. 19.

The experimental value is shown as a line, although the measured frequency can differ from the linear relationship by as much as 3 %. Generally, at higher velocities there is good agreement between the simulated and measured values. Interestingly, in the case of no paddle installed (not

further discussed here) the frequency is quite different from the experimentally determined one, but it displays the best linearity. The relatively good agreement of the two-dimensional results with the experiment is unexpected since the real flow is, of course, highly three-dimensional.

Summary
The present simulations were carried out for a number of cases representing deviations from a preferred design due to manufacturing tolerances.

The deviations of the characteristic frequencies from the design case are significant for the accuracy of the vortex flow meter, but it should be remembered that in frequency domain, in all the cases considered in the present study the main frequency displayed a clean peak, making its detection feasible. After proper calibration of the individual meters, the original accuracy can be recovered and the meters would deliver precise measurement, again. Only the case of the shifted paddle is somewhat more critical. Here, the amplitude of the low frequency disturbance is approaching the amplitude of the characteristic frequency and could be possibly dominating, making corresponding adjustments or modifications of the meter necessary.

Further research, in particular three-dimensional simulations, are necessary to shed more light on this behaviour.

References:

[1] C. Fureby, „Large-eddy simulation of turbulent anisochoric flows“, AIAA Journal, Vol. 33, No. 7, pp. 1263-1272, 1995.

[2] Hans, V., Poppen, G., Lavante, E. v., Perpeet, S., „Interaction between vortices and ultrasonic waves in vortex-shedding flow meters“, FLUCOME '97, Hayama, 1997.

[3] Hans, V., Poppen, G., Lavante, E. v., Perpeet, S., „Vortex-shedding flow meters and ultrasound detection: signal processing and bluff body geometry“, Flow Measurement and Instrumentation 9, pp. 79-82, 1998.

[4] Johnson, M.W., „Computation of flow in a vortex-shedding flow meter“, Flow Measurement and Instrumentation, pp. 201-208, 1990 .

[5] Madabhushi, R.K., Choi, D., Barber, T.J., „Unsteady simulations of turbulent flow behind a triangular bluff body“, AIAA Paper, pp. 97-3182, 1997.

[6] von Lavante, E., Yao, J. and Perpeet, S., „Effects of Disturbed Inflow on Vortex-Shedding from a Bluff Body“, AIAA paper 2000-2220, 2000.